

# Probing liquation cracking and solidification through modeling of momentum, heat, and solute transport during welding of aluminum alloys

S. Mishra, S. Chakraborty,<sup>a)</sup> and T. DebRoy<sup>b)</sup>

*Department of Materials Science and Engineering, The Pennsylvania State University, University Park, Pennsylvania 16802-5005*

(Received 8 November 2004; accepted 11 February 2005; published online 21 April 2005)

A transport phenomena-based mathematical model is developed to understand liquation cracking in weldments during fusion welding. Equations of conservation of mass, momentum, heat, and solute transport are numerically solved considering nonequilibrium solidification and filler metal addition to determine the solid and liquid phase fractions in the solidifying region and the solute distribution in the weld pool. An effective partition coefficient that considers the local interface velocity and the undercooling is used to simulate solidification during welding. The calculations show that convection plays a dominant role in the solute transport inside the weld pool. The predicted weld-metal solute content agreed well with the independent experimental observations. The liquation cracking susceptibility in Al–Cu alloy weldments could be reliably predicted by the model based on the computed solidifying weld-metal composition and solid fraction considering nonequilibrium solidification. © 2005 American Institute of Physics. [DOI: 10.1063/1.1886272]

## I. INTRODUCTION

Liquation cracking is a common problem in the fusion welding of aluminum alloys. In recent decades, the application of numerical transport phenomena has provided useful information about the thermal cycles and weld pool geometry in both linear and spot welding.<sup>1–19</sup> Computed temperatures have been used to understand the evolution of phase composition,<sup>5,16</sup> grain structure,<sup>7,8</sup> inclusion structure,<sup>17</sup> and weld-metal composition change owing to both the evaporation of alloying elements and the dissolution of gases.<sup>9,14</sup> However, these powerful transport phenomena-based modeling tools have not been used to understand weld solidification and liquation cracking in aluminum alloys.

Liquation cracking, also known as edge-of-weld cracking, base metal cracking, hot cracking, and heat-affected zone (HAZ) cracking, occurs in the HAZ when low melting point region, i.e., partially melted zone (PMZ), is formed during welding. Cracks form when the PMZ cannot withstand the tensile stresses generated during solidification.<sup>20</sup> The occurrence of liquation cracking in aluminum alloys has been confirmed by experiments.<sup>20–30</sup> Huang and Kou<sup>20</sup> found that the PMZ becomes prone to liquation cracking when the solid fraction in the PMZ becomes lower than that in the aluminum alloy weld metal. They argued that lower solid fraction in the PMZ makes this region weaker than the weld metal, making the PMZ vulnerable to liquation cracking.

Composition of the weld metal results from the mixing of the base metal with the filler metal. Solutes are distributed within the weld pool by convection and diffusion. Furthermore, both the thermodynamics and the kinetics of solidification affect the solute partitioning during solidification.

Both the partitioning of the solute and the mixing of the filler metal with the base metal need to be considered to understand the solidification process during welding. However, many previous attempts to understand weld pool solidification considered thermal field alone<sup>13,15</sup> and ignored the convective solute transport in the weld pool. Chakraborty and Dutta<sup>31</sup> developed a solidification model for studying heat and mass transfer in a single-pass laser surface alloying process. However, they<sup>31</sup> assumed equilibrium at the solid-liquid interface that may not be attained when the interface speed is comparable with or faster than the diffusion speed. Both the velocity of solidification front and the undercooling must be considered to accurately represent solidification during welding. The complex coupling of momentum, heat, and solute transport under nonequilibrium conditions during fusion welding has not been investigated. Such an approach is desirable for accurate prediction of the evolution of the solute concentration and improved understanding of the weldment solidification structure.

The goal of the research presented here is to understand the solute concentration field and the solidification process considering filler metal addition, fluid flow, and solute transport in the weld pool and nonequilibrium solidification. The model predictions of liquation cracking susceptibility in various aluminum alloy weldments based on Huang and Kou criterion are compared with the results of independent experimental studies to assess the capability of the model.

## II. MATHEMATICAL MODEL

The gas metal arc welding (GMAW) process considered involves a heat source that moves along the negative  $x$  direction with a constant speed,  $U$ . The welding arc heats the work piece surface and contributes to the formation of a molten pool. The filler metal melts and mixes with the molten base metal by convection and diffusion. As the heat

<sup>a)</sup>Present address: Department of Mechanical Engineering, Indian Institute of Technology Kharagpur, Kharagpur 721302 India.

<sup>b)</sup>Electronic mail: debroy@psu.edu

source moves, solidification of the molten zone leads to the structure of the solidified metal. The following major assumptions are made in the model:

- (i) The molten metal is considered to be Newtonian and incompressible.
- (ii) The density variation in the calculation domain is ignored except for the calculation of the buoyancy force following Boussinesq's approximation.
- (iii) Momentum transfer into the molten pool due to filler material addition is neglected for simplicity.
- (iv) Since the variation of surface tension with temperature is much larger than the variation of surface tension with solute concentration, the compositional dependence of the surface tension of the alloy is ignored.
- (v) For simplicity, a pseudobinary equivalent of the multicomponent alloy is considered for solidification modeling.

In a stationary coordinate system, the generalized governing equation for the transport of various quantities in the molten pool and its surroundings  $(x', y, z)$  can be written as

$$\frac{\partial}{\partial t}(\rho\phi) + \nabla(\rho\mathbf{u}\phi) = \nabla(\Gamma\nabla\phi) + S_\phi, \quad (1)$$

where  $t$  is time,  $\rho$  is the density,  $\phi$  is any dependent scalar variable per unit mass,  $\mathbf{u}$  is the resultant velocity vector,  $\Gamma$  is a generalized diffusion coefficient, and  $S_\phi$  is a source term. However, the transport phenomena inside the molten pool can be conveniently studied with respect to a coordinate system that moves along the  $x$  direction with the moving heat source by considering the following coordinate transformation:

$$x = x' - (-U)t, \quad (2)$$

where  $U$  is the welding speed along the negative  $x$  direction and  $x, y, z$  are coordinates in a frame moving with the welding torch. Henceforth, the following tensorial notation will be followed for description of the conservation equations,

$$x_1 = x, \quad x_2 = y, \quad x_3 = z. \quad (3)$$

Applying the above transformation and substituting  $\phi$  by the appropriate variables, the governing equations in the moving coordinate system assume the following forms.

### A. Conservation of mass (continuity equation)

The single-phase continuity equation for an incompressible fluid is given by

$$\frac{\partial u_i}{\partial x_i} = 0. \quad (4)$$

### B. Conservation of linear momentum

The equivalent single-phase linear momentum conservation equation for the  $x$  direction, with  $i=1, 2,$  and  $3$  in index notation is given by

$$\begin{aligned} \rho \frac{\partial u_x}{\partial t} + \rho \frac{\partial u_i u_x}{\partial x_i} = & -\frac{\partial p}{\partial x} + \frac{\partial}{\partial x_i} \left( \mu \frac{\partial u_x}{\partial x_i} \right) + \rho g \beta_T (T - T_r) \\ & + \rho g \beta_c (C - C_r) - \rho U \frac{\partial u_i}{\partial x_i} + S_x, \end{aligned} \quad (5)$$

where  $g$  is the gravitational acceleration,  $T_r$  is a reference temperature taken as the melting point of the solvent,  $T_m$ , and  $C_r$  is the concentration of the solute at  $T_r$ . The terms  $\beta_T$  and  $\beta_c$  represent the thermal and solutal volumetric expansion coefficients, respectively. The source term  $S_x$  considers frictional resistance to flow experienced by the liquid metal in the two-phase solid-liquid region similar to flow in a porous medium. This resistance is calculated using Darcy's model and the Carman-Kozeny relationship.<sup>13,18,32</sup> The source term also includes the Lorentz force as a consequence of the electric current used in the welding. Combining these two effects, the source term can be represented as

$$S_x = -\frac{K_m(1-f_l)^2}{f_l^3 + b} u_x + (J \times B)_x, \quad (6)$$

where  $f_l$  is the liquid fraction given as  $f_l = \Delta H / L$ , where  $\Delta H$  is the latent heat content of a control volume,  $L$  is the latent heat of fusion,  $J$  is the current density, and  $B$  is the magnetic-field intensity. In Eq. (6),  $K_m$  is a large number<sup>13</sup> and  $b$  is a small number to avoid division by zero. The above formulation ensures that the velocity becomes zero in the solid region and increases continuously into the liquid region. The details of the formulation of the above term have been reported by Brent *et al.*<sup>32</sup> and the calculation of the Lorentz force term is presented elsewhere,<sup>11</sup> and these are not repeated here.

### C. Conservation of energy

The thermal energy conservation equation is given by

$$\begin{aligned} \rho \frac{\partial h}{\partial t} + \rho \frac{\partial (u_i h)}{\partial x_i} = & \frac{\partial}{\partial x_i} \left( K \frac{\partial T}{\partial x_i} \right) - \rho \frac{\partial (\Delta H)}{\partial t} - \rho \frac{\partial (u_i \Delta H)}{\partial x_i} - S_d \\ & - \rho U \frac{\partial h}{\partial x_i} - \rho U \frac{\partial \Delta H}{\partial x_i}, \end{aligned} \quad (7)$$

where  $K$  is the thermal conductivity and  $\Delta H$  is the latent enthalpy content of the computational cell under consideration given by the following expression:

$$\begin{aligned} \Delta H = L & \quad \text{if } T > T_l \\ = f_l L & \quad \text{if } T_s \leq T < T_l \\ = 0 & \quad \text{if } T < T_s, \end{aligned} \quad (8)$$

where  $T_s$  and  $T_l$  are the solidus and liquidus temperatures, respectively. In Eq. (7), the term  $S_d$  represents a volumetric heat source term due to the addition of hot metal droplets from the melting electrode. Calculation of this term is described in detail in a recent paper.<sup>2</sup>

## D. Species conservation and solidification

The general form of species conservation equation is given by

$$\frac{\partial(\rho C)}{\partial t} + \frac{\partial(\rho u_i C)}{\partial x_i} = \frac{\partial}{\partial x_i} \left( \rho D \frac{\partial C}{\partial x_i} \right) - \rho U \frac{\partial C}{\partial x_i}, \quad (9)$$

where  $C$  is the solute concentration and  $D$  is the effective-mass diffusivity of the solute. The variable  $C$  embodies components from both solid and liquid phases. Voller *et al.*<sup>33</sup> have shown that Eq. (9) may be rewritten in terms of liquid phase concentration,  $C_l$ , and nonequilibrium partition coefficient. Following their approach and neglecting diffusion in solid, Eq. (9) may be rewritten as<sup>33</sup>

$$\begin{aligned} \frac{\partial}{\partial t}(\rho C_l) + \frac{\partial(\rho u_i C_l)}{\partial x_i} &= \frac{\partial}{\partial x_i} \left( \rho f_l D_l \frac{\partial C_l}{\partial x_i} \right) + \frac{\partial}{\partial t}(\rho f_s C_l) \\ &- K_p C_l \frac{\partial}{\partial t}(\rho f_s) - \rho U \frac{\partial C_l}{\partial x_i} - S_m, \quad (10) \end{aligned}$$

where  $K_p$  is the partition coefficient. In Eq. (10),  $D_l$  is an effective diffusion coefficient to be described subsequently,  $f$  denotes the appropriate phase fraction with subscripts  $l$  and  $s$  referring to liquid and solid phases, respectively, and  $S_m$  is a time-averaged volumetric mass source term to incorporate the filler metal addition.

Since the solute partitioning at the solid-liquid interface may not reach thermodynamic equilibrium, calculations of  $f_s$  and  $f_l$  and the prescription of an appropriate partition coefficient in Eq. (10) require a rigorous nonequilibrium solidification model. Equation (10) also indicates a strong coupling among the thermal, solutal, and velocity fields. A key factor in this coupling is the appropriate modeling of the liquid fraction that affects the orientation and location of the pool boundaries. The iterative updating of liquid fraction (or, equivalently, nodal enthalpy) is done in the entire concentration field, since the enthalpy and concentration fields are coupled through the nonequilibrium solidification kinetics at the interface.

## E. Filler metal addition

Filler metal addition to the weld pool is considered by incorporating time-averaged volumetric heat and mass sources in the enthalpy and solute conservation equations. The volumetric heat source is characterized by its radius ( $R_v$ ), height ( $d$ ), and power density ( $S_v$ ) and considers the interaction between metal droplets and weld pool for various welding conditions.<sup>2,3</sup> The radius of the volumetric heat source is assumed to be 2.7 times the droplet radius,<sup>19</sup> and the height ( $d$ ) is calculated from the following equation based on energy balance:

$$d = h_v - x_v + D_d, \quad (11)$$

where  $h_v$  is the estimated height of cavity by the impact of metal droplets,  $x_v$  is the distance traveled by the center of the slug between the impingement of two successive droplets, and  $D_d$  is the droplet diameter. The total sensible heat input from the metal droplets,  $Q_t$ , is given as

$$Q_t = \rho \pi r_w^2 w_f H_d, \quad (12)$$

where  $\rho$  is the density,  $r_w$  is the radius of the wire,  $w_f$  is the wire feeding rate, and  $H_d$  is the total enthalpy of the droplets. It should be noted that a portion of  $Q_t$  is used to heat the additional metal from the droplets up to liquidus temperature. Therefore, the effective heat of droplets ( $Q_d$ ) carried into the weld pool is given as

$$Q_d = \rho \pi r_w^2 w_f C_{pl}(T_d - T_l), \quad (13)$$

where  $C_{pl}$  is the specific heat of the liquid metal,  $T_d$  is the droplet temperature, and  $T_l$  is the liquidus temperature.

The values of  $h_v$  and  $x_v$  in Eq. (11) are calculated based on energy balance as

$$h_v = \left( -\frac{2\gamma}{D_d \rho g} + \sqrt{\left[ \left( \frac{2\gamma}{D_d \rho g} \right)^2 + \frac{D_d v_d^2}{6g} \right]} \right), \quad (14)$$

$$x_v = \left( h_v + \frac{2\gamma}{D_d \rho g} \right) \left\{ 1 - \cos \left[ \left( \frac{g}{h_v} \right)^{1/2} \Delta t \right] \right\}, \quad (15)$$

where  $\gamma$  is the surface tension of the molten metal,  $g$  is the acceleration due to gravity,  $v_d$  is the droplet impingement velocity, and  $\Delta t$  is the interval between two successive drops ( $\Delta t = 1/f$ , where  $f$  is the droplet transfer frequency). As shown in Eqs. (11)–(15), the calculation of the dimensions of the volumetric heat source requires the knowledge of the droplet transfer frequency, radius, and impingement velocity. These parameters are determined from the correlations available in the literature.<sup>2</sup> From the computed values of  $Q_d$ ,  $D_d$ , and  $d$ , the time-averaged power density for grid points within the volumetric heat source,  $S_d$ , is calculated as

$$S_d = \frac{Q_d}{\pi D_d^2 d}. \quad (16)$$

Solute addition from the filler metal is considered by incorporating a time-averaged volumetric mass source term,  $S_m$ , in the solute conservation equation, Eq. (10). The dimensions of the volumetric mass source are assumed to be the same as the volumetric heat source. The net mass of solute from the metal droplets,  $Q_t$ , is given as

$$Q_t = \rho \pi r_w^2 w_f (C_f - C), \quad (17)$$

where  $\rho$  is the density,  $r_w$  is the radius of the wire,  $w_f$  is the wire feeding rate,  $C_f$  is the concentration of solute in the filler metal drops, and  $C$  is the local solute concentration. The time-averaged volumetric mass source,  $S_m$ , for grid points within the mass source region is given by

$$S_m = \frac{Q_t}{\pi D_d^2 d}. \quad (18)$$

## F. Thermosolutal-flow coupling

### 1. Enthalpy updating

The following iterative enthalpy updating scheme proposed by Brent *et al.*<sup>32</sup> is chosen in the present study for its adaptability in a fixed-grid enthalpy based framework:

$$[\Delta H_P]_{n+1} = [\Delta H_P]_n + \frac{a_p}{a_p^0} \lambda [\{h_p\}_n - F^{-1}\{\Delta H_P\}_n], \quad (19)$$

where  $a_p$  and  $a_p^0$  are the coefficients of enthalpy for the nodal point  $P$  in the discretized energy equation for the current and the previous time steps, respectively,<sup>34</sup>  $\Delta H_P$  is the latent heat content,  $h_p$  is the sensible enthalpy associated with the nodal point  $P$ ,  $n$  is the number of iterations,  $\lambda$  is a relaxation factor, and  $F^{-1}$  is a suitable function that relates local enthalpy with temperature and liquid fraction. In order to include the appropriate thermosolutal effects<sup>35</sup> in  $F^{-1}$ , the interfacial temperature,  $T$ , is represented as a function of local liquidus composition,  $C_l$ , as<sup>36</sup>

$$T = T_m + m_L C_l - V/\beta_0 - \Gamma \kappa, \quad (20)$$

where  $T_m$  is the melting point of the solvent,  $m_L$  is the non-equilibrium liquidus-line slope described by Eq. (21),  $V$  is the normal interface velocity,  $\beta_0$  is a kinetic coefficient of interface motion,  $\Gamma$  is a capillary constant calculated as  $\Gamma = T_m \gamma / L \rho$ ,  $\gamma$  is the surface tension,  $L$  is the latent heat of freezing,  $\rho$  is the density, and  $\kappa$  is the mean curvature of the solid-liquid interface. Equation (20) represents a deviation of the interfacial temperature from its local equilibrium value due to motion of the interface, the local interfacial curvature-undercooling effect, and the nonequilibrium partitioning of the solute. The partitioning effect is considered by relating the nonequilibrium liquidus-line slope ( $m_L$ ) in Eq. (20) with its equilibrium value ( $m_L^*$ ) as<sup>36,37</sup>

$$m_L = m_L^* \left( 1 + \frac{1}{1 - k_p^*} \{k_p^* - k_p [1 - \ln(k_p/k_p^*)]\} \right), \quad (21)$$

where  $k_p$  is the modified partition coefficient that can be expressed in terms of equilibrium partition coefficient,  $k_p^*$ , as<sup>36</sup>

$$k_p = \begin{cases} \frac{k_p^* [1 - (V/V_D^L)^2] + V/V_D^L}{1 - (V/V_D^L)^2 + V/V_D^L}, & \dots, \text{ for } V < V_D^L \\ 1, & \dots, \text{ for } V \geq V_D^L. \end{cases} \quad (22)$$

In Eq. (22),  $V_D^L$  is the diffusive speed in the liquid, which can be calculated as<sup>36</sup>

$$V_D^L = (D_l^*/\tau_D^L)^{0.5}, \quad (23)$$

where  $\tau_D^L$  refers to the time of diffusional relaxation of collective atoms (molecules, particles) to their equilibrium state in a local volume of alloy.<sup>36</sup> The diffusive speed at which a solute atom diffuses through the interfacial region can be approximated by the ratio of diffusivity of the solute atoms at the interface and a length scale characterizing the interface width. Furthermore, the interface velocity ( $V$ ) in Eq. (22) can be calculated in an iterative manner using the following equation:<sup>13</sup>

$$V = \frac{k_S G_S - k_L G_L}{f_l L}, \quad (24)$$

where  $G_S$  and  $G_L$  are the temperature gradients in solid and mushy zone at the mushy zone/solid interface, respectively,  $k_S$  and  $k_L$  are thermal conductivities of the solid and liquid phases, respectively,  $f_l$  is the liquid fraction, and  $L$  is the

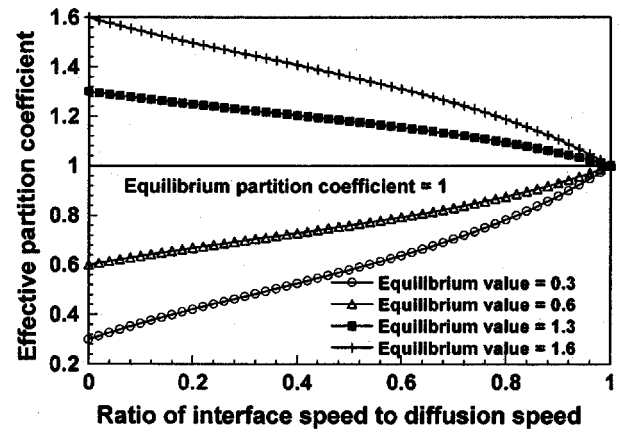


FIG. 1. Effect of interface speed on local interfacial partitioning.

latent heat of freezing. For a known interface velocity, the diffusion coefficient appearing in Eq. (10) can be prescribed as<sup>36</sup>

$$D_l = D_l^* [1 - (V/V_D^L)^2], \dots, \text{ for } V < V_D^L \\ = 0, \dots, \text{ for } V \geq V_D^L, \quad (25)$$

where  $D_l^*$  is the diffusion coefficient in the liquid under the conditions of interfacial equilibrium.

The impact of high solidification rate on local interfacial temperature, as indicated by Eqs. (21) and (22), is worth examining at this point. From Fig. 1, it can be observed that the difference between solidus and liquidus compositions progressively diminishes with an increase of interface velocity due to lack of time available for atomistic rearrangements. Ultimately, as the interface velocity approaches the diffusive speed, the partition coefficient tends to unity. The resulting effect on solidus- and liquidus-line slopes is depicted in Fig. 2. It can be observed from this figure that with an increase in the interface speed, the difference between the liquidus- and solidus-line slopes decreases rapidly. Thus, the effective solidification range becomes progressively smaller at faster solidification rates. The solidus and liquidus temperatures tend to coincide as the diffusive speed limit is ap-

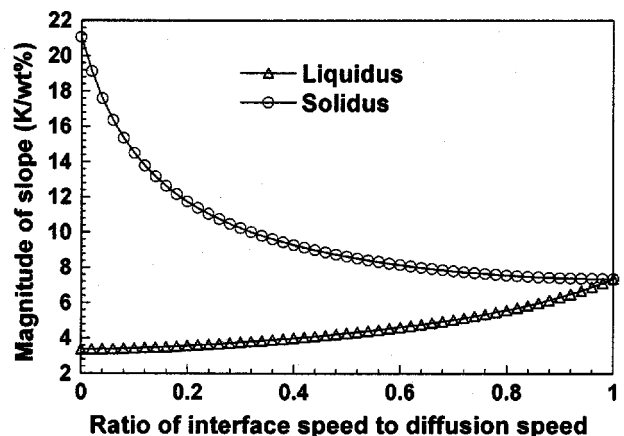


FIG. 2. Effect of interface speed on solidus- and liquidus-line slopes (an equilibrium liquidus slope of  $-3.37$  K/wt% and an equilibrium partition coefficient of 0.16 were chosen for this specific demonstration).

proached. The mushy zone virtually disappears and the liquid instantaneously freezes to form solid crystals without passing through a freezing range. At high solidification rates, the solid fraction cannot be calculated based on equilibrium considerations.

Equations (21)–(24) can be effectively used to complete the iteration cycle involving updating of enthalpy using Eq. (19). The calculations require an appropriate functional relation between liquid composition,  $C_l$ , and liquid fraction,  $f_l$ , consistent with the local solute balance,

$$(C_l - C_s)df_s = (1 - f_s)dC_l, \quad (26)$$

where  $f_s$  is the mass fraction of the solid and  $C_s$  is the solid phase composition. Replacing  $f_s$  by  $(1 - f_l)$  in Eq. (26), where  $f_l$  is the mass fraction of the liquid, and integrating,  $f_l$  is obtained as

$$f_l = \exp \left\{ - \int_{C_0}^{C_l} \frac{dC_l}{C_l(1 - k_p)} \right\}, \quad (27)$$

where  $k_p$ , which replaces  $C_s/C_l$ , is a convection-corrected partition coefficient representing the nonequilibrium effects [given by Eq. (22)]. Equation (27) can be integrated if the variation of  $k_p$  with  $C_l$  is known. For the specific case of a composition-independent partition coefficient, integration of Eq. (27) gives<sup>38</sup>

$$C_l = C_0 f_l^{k_p - 1}, \quad (28)$$

where  $C_0$  is the initial composition of liquid. Although Eq. (28) appears similar in form to the well-known Scheil's equation,<sup>38</sup> a key difference lies in the fact that the partition coefficient in Eq. (28) is a strong function of the interface growth rate governed by Eq. (24) and not a constant.

With the aid of Eqs. (20) and (28), a final form of the enthalpy updating function appearing in Eq. (19) can now be obtained as

$$F^{-1}(\Delta H) = c_p \left[ T_m + m_L C_0 \left( \frac{\Delta H}{L} \right)^{(k_p - 1)} - V/\beta_0 - \Gamma \kappa \right]. \quad (29)$$

Finally, the liquid fraction is calculated by using Eq. (19) as

$$f_l = \frac{\Delta H}{L}. \quad (30)$$

Possible unrealistic intermediate estimates predicted by Eq. (30) during iterations can be avoided by imposing the following constraints:

$$\begin{aligned} f_l &= 0 \text{ if } f_l < 0 \\ &= 1 \text{ if } f_l > 1. \end{aligned} \quad (31)$$

## 2. Steps of enthalpy updating

Step 1. Initialize the velocity, temperature, concentration, and liquid fraction field.

Step 2. Form coefficients of the discretization equations for fluid flow, heat transfer, and mass transfer, and solve the resultant system of linear algebraic equations.

TABLE I. Data used in the calculations.

Problem data/physical property	Value <sup>a</sup>
Arc current (A)	140
Arc voltage (V)	22
Welding speed (m s <sup>-1</sup> )	4.2 × 10 <sup>-3</sup>
Density (kg m <sup>-3</sup> )	2400
Viscosity of liquid (kg m <sup>-1</sup> s <sup>-1</sup> )	0.3 × 10 <sup>-3</sup>
Specific heat (J kg <sup>-1</sup> K <sup>-1</sup> )	1.06 × 10 <sup>3</sup>
Mass diffusivity of copper in liquid aluminum (m <sup>2</sup> s <sup>-1</sup> ) under interfacial equilibrium conditions	3.0 × 10 <sup>-9</sup>
Thermal conductivity (W m <sup>-1</sup> K <sup>-1</sup> )	192
Equilibrium partition coefficient	0.16
Equilibrium slope of liquidus line (K/wt %)	-3.37
Solidus temperature of alloy 2219 (K)	821
Liquidus temperature of alloy 2219 (K)	911

<sup>a</sup>See Ref. 39.

Step 3. Calculate the ratio of interface speed to diffusive speed [using Eqs. (23) and (24)].

Step 4. Calculate the nonequilibrium partition coefficient at nodal points [using Eq. (22)].

Step 5. Calculate the nonequilibrium liquidus slope [using Eq. (21)].

Step 6. Update nodal latent enthalpy, and hence liquid fraction, as per Eqs. (19) and (30), respectively. This step leads to a corrected weld pool geometry based on the phase fraction evolution through appropriate nonequilibrium thermosolutal coupling.

Step 7. Go back to step 2, and iterate until convergence.

## G. Boundary conditions

The temperature and velocity boundary conditions are available in the literature<sup>13</sup> and are not repeated here. The boundary conditions for solute transport at the solidification interface need to consider nonequilibrium partitioning of solute at the solidification front,

$$C_l = C_w/k_p, \quad (32)$$

where  $C_l$  is the local solute concentration in the liquid and  $C_w$  is the solute concentration in the solidified weld metal. Similarly, the boundary condition at the melting front can be written as

$$C_l = C_b, \quad (33)$$

where  $C_b$  is the concentration of the solute in the base metal.

## III. RESULTS AND DISCUSSION

GMA welding of 2219 aluminum–copper alloy containing 6.3 wt % Cu was simulated. The filler metal compositions varied from 0.08 to 9.0 wt % Cu. The data used in the calculations are summarized in Table I. Figure 3 shows the computed velocity and temperature fields in the weld pool of 2219 alloy with the filler metal composition of 0.08 wt % Cu. The weld pool is wide and shallow because the aluminum alloy has a negative temperature coefficient of surface tension ( $d\gamma/dT$ ) which causes the liquid metal to move from the middle to the periphery on the weld pool surface. The

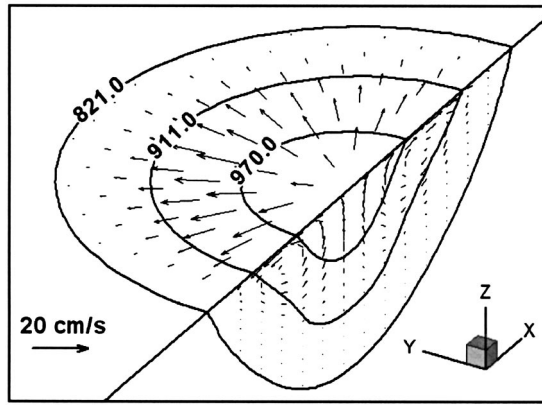


FIG. 3. Velocity and temperature fields in the weld pool for the welding conditions indicated in Table I. The filler metal concentration was 0.08 wt % copper. All the temperatures are in degree Kelvin.

relative importance of convection and conduction in the overall transport of heat in the weld pool can be assessed from the value of the Peclet number,  $Pe_h$ , which is given by

$$Pe_h = \frac{u\rho C_p L}{k}, \quad (34)$$

where  $u$  is the velocity,  $\rho$  is the density,  $C_p$  is the specific heat at constant pressure,  $L$  is the characteristic length, and  $k$  is the thermal conductivity of the melt. When  $Pe_h$  is large, which in physical terms means large melt velocity, large weld pool, and poor thermal conductivity, heat is transported primarily by convection. In the aluminum alloy welds, typical velocity in the pool is 0.2 m/s, density is 2400 kg/m<sup>3</sup>, specific heat is 1060 J/kg K, characteristic length is 0.0044 m, and thermal conductivity is 192 W/m K. The corresponding value of  $Pe_h$  is found to be 12, which is much larger than unity. This value of  $Pe_h$  indicates that heat is transported mainly by convection in the weld pool. Therefore, accurate calculations of temperature field can only be done by considering convective heat transport.

The Peclet number for mass transfer,  $Pe_m$ , indicates the relative importance of convection and conduction in the overall transport of solute in the weld pool.

$$Pe_m = \frac{uL}{D}, \quad (35)$$

where  $D$  is the mass diffusivity. The mass diffusivity of aluminum alloy is  $3.0 \times 10^{-9}$  m<sup>2</sup>/s. The corresponding value of  $Pe_m$  is calculated to be  $2.9 \times 10^5$ , which indicates that convection is the primary mode of mass transport in the weld pool. Therefore, it is necessary to consider convective mass transport in order to accurately predict the solute concentration distribution in the weld pool.

Figures 4(a)–4(d) show the computed solute concentration distributions within the weld pool for four filler metal compositions: 0.08, 2.0, 4.0, and 9.0 wt % Cu. It can be observed that convection plays a dominant role in solute distribution in the weld pool causing efficient mixing of the base metal with the filler metal. At the melting front, in front of the pool, the base metal melts and forms a liquid of the same composition. The filler metal then mixes with the liquid from

the base metal resulting in a weld-metal composition that lies between the filler metal and the base metal compositions. At the solidification front, the solute is rejected from the solidified material into the molten pool. As a result, high solute concentration is observed at the solidification front in Figs. 4(a)–4(d). Similarly, in the transverse sections ahead of the heat source, the composition near the melting front is the same as that of the base metal. However, in transverse sections behind the heat source, segregation of the solute is observed near the solidification front. In the middle of the weld pool, a large amount of filler metal is added and the solute concentration is fairly close to the filler metal composition. The solute concentrations at the melting and the solidification fronts have been further clarified in Fig. 5, where the computed solute concentration along the direction of motion of the torch is shown. It is noteworthy that the high solute content at the solidification front does not have as much influence on the overall concentration distribution as the mixing of the filler metal with the base metal. This behavior can be attributed to a very low-mass diffusivity of copper in the alloy and very low liquid velocities in the two-phase region adjacent to the solidification front. The rejected solute is confined to a very small region and the low velocities in the two-phase region prevent rapid mixing of the rejected solute into the weld pool.

Since the composition of a single-pass GMA aluminum weld is essentially uniform,<sup>20</sup> the solidified weld-metal solute concentration was assumed to be equal to the average concentration of the solute in the molten weld pool. As shown in Figs. 4 and 5, the concentration of solute in the solidified weld metal depends on the filler metal composition. The accuracy of the calculated weld-metal composition can be examined by comparing the computed weld-metal composition for 0.08 wt % filler metal addition with the corresponding independent experimental result of Huang and Kou.<sup>20</sup> For a GMA weld of 2219 alloy using a filler metal containing 0.08 wt % copper, Huang and Kou<sup>20</sup> measured the weld-metal composition to be 3.43 wt % copper. For the same welding conditions, the computed weld-metal composition was equal to 3.17 wt % copper, as shown in Figs. 4(a) and 5, thus confirming the accuracy of the calculations. The results also indicate the importance of solute transport by convection. Accurate solute concentration distribution cannot be calculated by considering only the diffusive transport.

Gittos and Scott<sup>40</sup> proposed that liquation cracking occurs when the base metal solidus temperature is below the weld-metal solidus temperature. In other words, if the base metal solute content is higher than that of the weld metal, then the PMZ is susceptible to liquation cracking. Figure 6 is a plot of the computed wt % Cu in the weld metal versus the wt % Cu in the filler metal. The concentration of Cu in the base metal was 6.3 wt %. Thus, based on the criterion proposed by Gittos and Scott,<sup>40</sup> the PMZ becomes susceptible to liquation cracking when the weld-metal concentration is lower than 6.3 wt % Cu. However, Huang and Kou<sup>20</sup> argued that the cooling rate during welding may be too high for equilibrium solidification to occur, and solidification can continue far below the equilibrium solidus temperature. They<sup>20</sup> proposed the criterion that the PMZ becomes prone

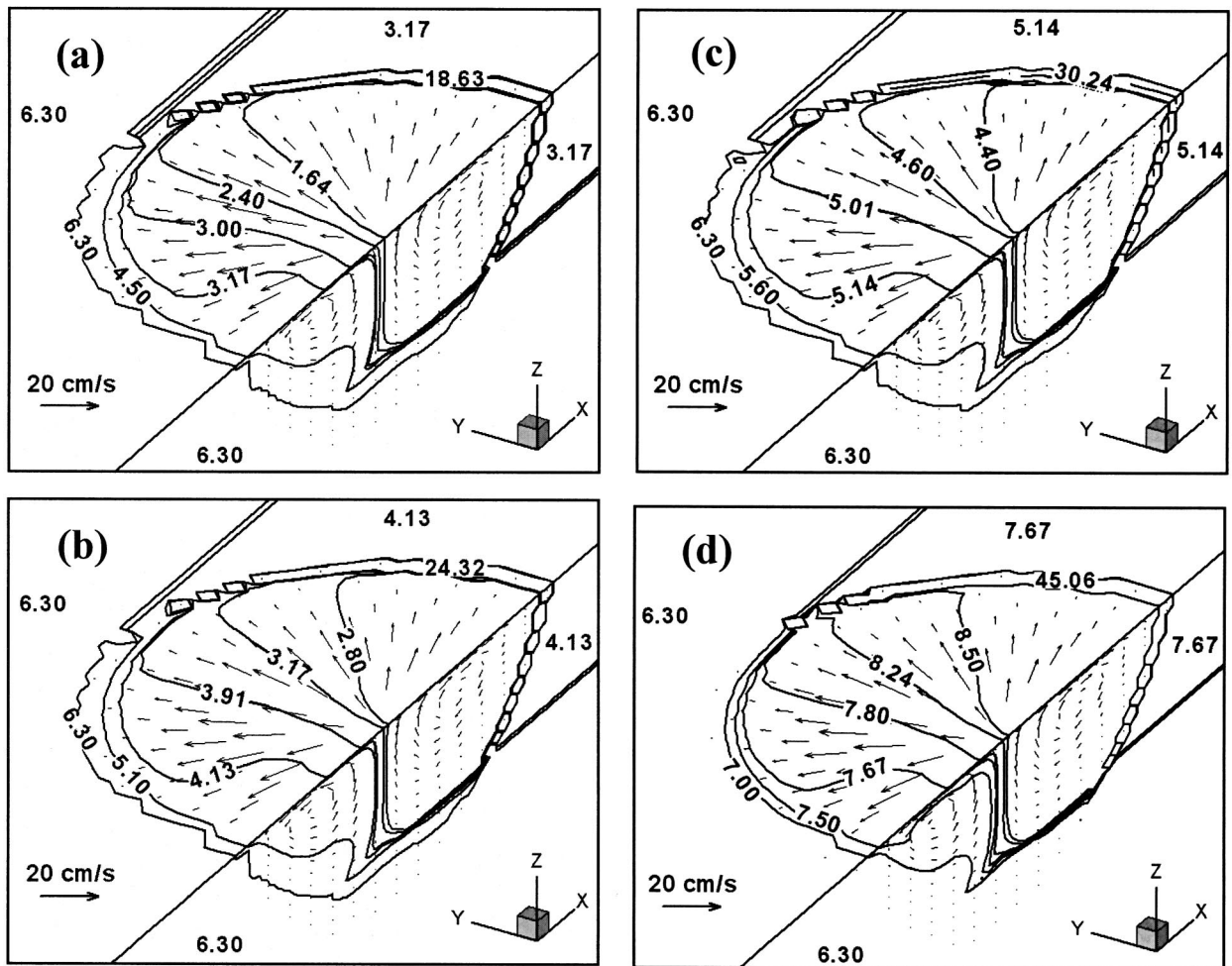


FIG. 4. Concentration field (wt % Cu) in the weld pool. The filler metal compositions were (a) 0.08, (b) 2.0, (c) 4.0, and (d) 9.0 wt % Cu.

to liquation cracking when the solid fraction in the PMZ becomes lower than that of the weld metal. A weaker PMZ with lower solid fraction makes this region vulnerable to liquation cracking. Calculation of the solid fraction in the solidifying region requires the computed values of nonequilibrium partition coefficient, which is shown in Fig. 7. It should be noted that the value of the nonequilibrium partition

coefficient is higher than that of the equilibrium value. The higher value is consistent with the shrinking of the two-phase region at high solidification rates. Once  $k_p^*$  and  $k_p$  were obtained for each temperature, Eq. (21) was used to get the slope of the liquidus line ( $m_l$ ) at these temperatures. Next,

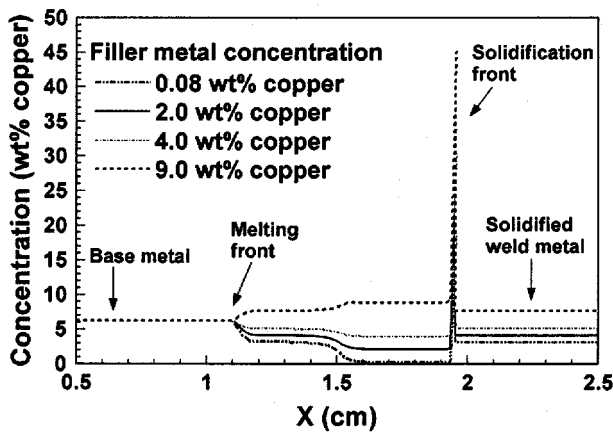


FIG. 5. The concentration of copper (wt %) in the weld along the direction of motion of the torch. The base metal composition was 6.3 wt % copper.

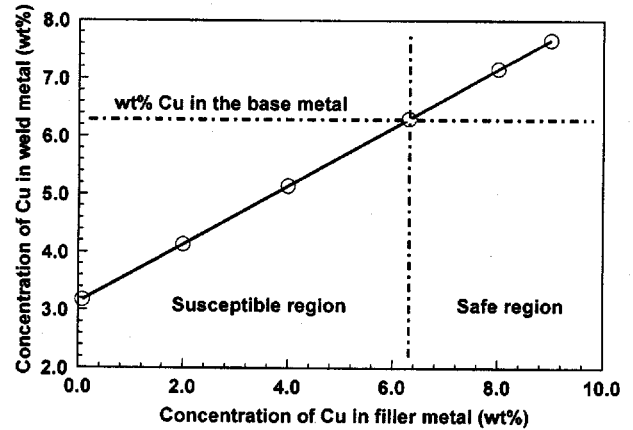


FIG. 6. The concentration of copper in the weld metal for different filler metal compositions. The concentration of copper in the base metal was 6.3 wt %. The safe and susceptible regions are indicated for equilibrium solidification.

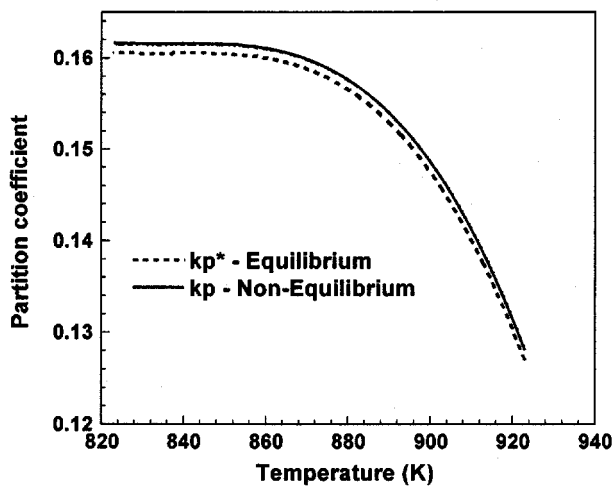


FIG. 7. Variation of equilibrium partition coefficient ( $k_p^*$ ) and nonequilibrium partition coefficient ( $k_p$ ) with temperature.

the modified liquidus composition ( $C_l$ ) at each temperature was calculated using  $k_p$ ,  $m_l$ , and the melting point of pure aluminum, 933 K. The corresponding values of the modified solidus compositions,  $C_s$ , at each temperature could be obtained from the values of  $k_p$  and  $C_l$  at these temperatures. The modified  $C_s$  and  $C_l$  were then used to calculate the nonequilibrium solid fractions. The computed solid fraction for the 2219 alloy, having 6.3 wt % Cu taking into account the nonequilibrium solidification, is shown in Fig. 8. The solid line curve in Fig. 8 was calculated from the equilibrium phase diagram using the equilibrium  $C_s$  and  $C_l$  values. The nonequilibrium solid fraction is lower than the corresponding equilibrium value because of undercooling which prevents solidification to occur at equilibrium temperature at high solidification rates.

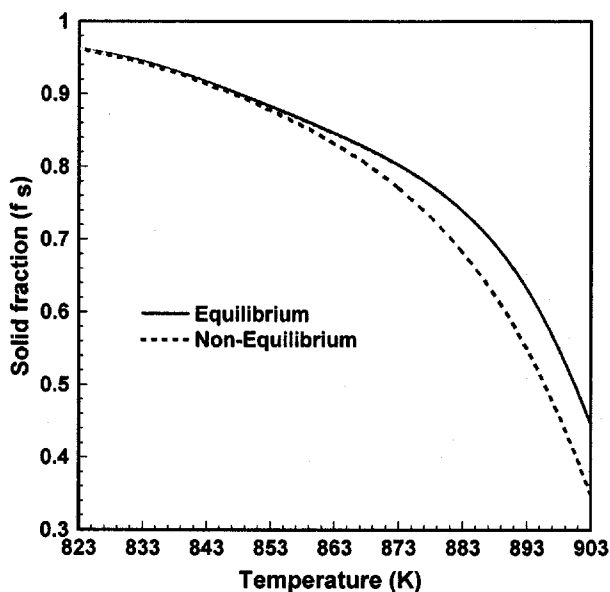


FIG. 8. Solid fraction vs temperature for alloy composition of 6.3 wt % copper. The solid line curve was obtained from the equilibrium phase diagram and the dotted line curve was obtained using the modified nonequilibrium solidus and liquidus lines.

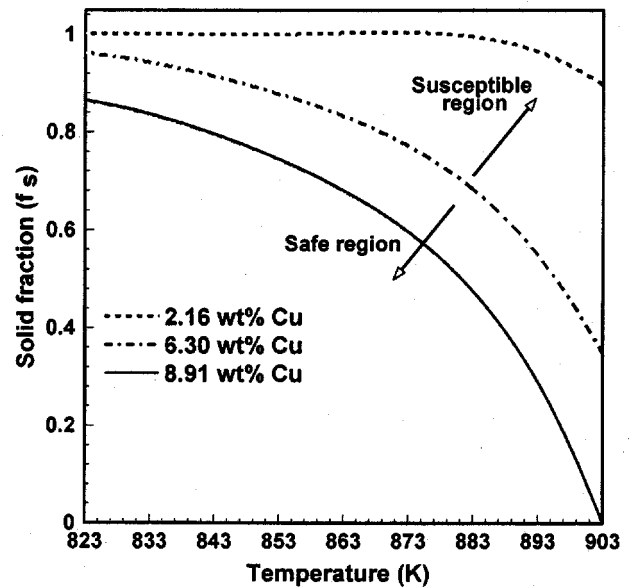


FIG. 9. Solid fraction vs temperature calculated using modified nonequilibrium solidus and liquidus lines for different alloy compositions. The PMZ composition was 6.3 wt % Cu. The calculated mushy zone compositions, or the solidifying weld-metal compositions, of 2.16 and 8.91 wt % Cu correspond to the filler metal compositions of 2.0 and 9.0 wt % Cu, respectively.

The variation of nonequilibrium solid fraction with temperature for three cases has been plotted in Fig. 9. One plot is for the base metal or the PMZ composition, i.e., 6.3 wt % Cu, and the other two are for the solidifying weld-metal compositions in the mushy region computed from the solute transport model for two welding conditions. The lower plot represents welding of 2219 alloy using a filler metal with 9.0 wt % Cu that leads to a mushy zone composition of 8.91 wt % Cu for the wire feed rates and other parameters indicated in Table I. Similarly, the upper plot indicates the use of a filler metal of 2.0 wt % Cu, for the same welding conditions, that leads to a mushy zone composition of 2.16 wt % Cu. The solid fraction in the PMZ can be compared with that in the solidifying region, i.e., the mushy zone. The lower graph representing 9.0 wt % Cu-containing filler metal has a lower solid fraction in the mushy zone than in the PMZ. Therefore, the solidifying weld metal has a lower strength than the PMZ and the PMZ is not susceptible to liquation cracking. In contrast, when the 2.0 wt % Cu-containing filler metal is used, the solid fraction in the solidifying metal is higher than that in the PMZ. Consequently, the solidifying weld metal is stronger than the PMZ, making the PMZ susceptible to liquation cracking. Thus, the present calculations considering convective solute transport, nonequilibrium solidification, and filler metal addition can be used to predict liquation cracking susceptibility in aluminum alloy welds.

#### IV. CONCLUSIONS

A numerical model that considers momentum, heat, and solute transport has been developed to understand nonequilibrium solidification in welds. The model uses an effective partition coefficient that considers both the local interface

velocity and the undercooling to simulate solidification during welding. The computed concentration profiles reflect the dissolution of the base metal at the melting front, the strong convection in the weld pool, mixing of the filler metal with the base metal, and solute rejection at the solidifying interface. The calculations showed that convection plays a dominant role in solute transport in the weld pool and diffusion calculations alone are insufficient. The predicted weld-metal solute content agreed well with the independent experimental observations. Using the computed average composition in the two-phase mushy region, the solid fraction in the solidifying weld metal was compared with that in the PMZ for various filler metal compositions. In each case, the susceptibility of liquation cracking was determined by Huang and Kou's criteria, i.e., by comparing the solid fraction in the solidifying weld metal with the corresponding value in the PMZ. The model predictions of liquation cracking susceptibility in Al-Cu alloy weldments were confirmed by independent experiments for various filler metal compositions.

## ACKNOWLEDGMENTS

This research was supported by a grant from the U.S. Department of Energy, Office of Basic Energy Sciences, Division of Materials Sciences, under Grant No. DE-FGO2-01ER45900. The authors thank Xiuli He, Amit Kumar, Rituraj Nandan, and Rohit Rai for their comments during the preparation of this manuscript.

<sup>1</sup>H. Zhao and T. DebRoy, *J. Appl. Phys.* **93**, 10089 (2003).

<sup>2</sup>W. Zhang, C.-H. Kim, and T. DebRoy, *J. Appl. Phys.* **95**, 5210 (2004).

<sup>3</sup>W. Zhang, C.-H. Kim, and T. DebRoy, *J. Appl. Phys.* **95**, 5220 (2004).

<sup>4</sup>A. De and T. DebRoy, *J. Appl. Phys.* **95**, 5230 (2004).

<sup>5</sup>J. W. Elmer, T. A. Palmer, S. S. Babu, W. Zhang, and T. DebRoy, *J. Appl. Phys.* **95**, 8327 (2004).

<sup>6</sup>A. De and T. DebRoy, *J. Phys. D* **37**, 140 (2004).

<sup>7</sup>S. Mishra and T. DebRoy, *J. Phys. D* **37**, 2191 (2004).

<sup>8</sup>S. Mishra and T. DebRoy, *Acta Mater.* **52**, 1183 (2004).

<sup>9</sup>X. He, P. Fuerschbach, and T. DebRoy, *J. Appl. Phys.* **94**, 6949 (2003).

<sup>10</sup>C.-H. Kim, W. Zhang, and T. DebRoy, *J. Appl. Phys.* **94**, 2667 (2003).

<sup>11</sup>A. Kumar and T. DebRoy, *J. Appl. Phys.* **94**, 1267 (2003).

<sup>12</sup>S. A. David, R. Trivedi, M. E. Eshelman, J. M. Vitek, S. S. Babu, T. Hong, and T. DebRoy, *J. Appl. Phys.* **93**, 4885 (2003).

<sup>13</sup>W. Zhang, G. G. Roy, J. W. Elmer, and T. DebRoy, *J. Appl. Phys.* **93**, 3022 (2003).

<sup>14</sup>X. He, P. Fuerschbach, and T. DebRoy, *J. Phys. D* **36**, 3079 (2003).

<sup>15</sup>X. He, P. W. Fuerschbach, and T. DebRoy, *J. Phys. D* **36**, 1388 (2003).

<sup>16</sup>J. W. Elmer, T. A. Palmer, W. Zhang, B. Wood, and T. DebRoy, *Acta Mater.* **51**, 3333 (2003).

<sup>17</sup>T. Hong and T. DebRoy, *Metall. Mater. Trans. B* **34**, 267 (2003).

<sup>18</sup>K. Mundra, T. DebRoy, and K. Kelkar, *Numer. Heat Transfer, Part A* **29**, 115 (1996).

<sup>19</sup>A. Kumar and T. DebRoy, *Int. J. Heat Mass Transfer* **47**, 5793 (2004).

<sup>20</sup>C. Huang and S. Kou, *Weld. J. (Miami, FL, U. S.)* **83**, 50s (2004).

<sup>21</sup>H. Zhao and T. DebRoy, *Metall. Mater. Trans. B* **32**, 163 (2001).

<sup>22</sup>H. W. Kerr and M. Katoh, *Weld. J. (Miami, FL, U. S.)* **66**, 251s (1987).

<sup>23</sup>M. Miyazaki, K. Nishio, M. Katoh, S. Mukae, and H. W. Kerr, *Weld. J. (Miami, FL, U. S.)* **69**, 362s (1990).

<sup>24</sup>C. Huang and S. Kou, *Weld. J. (Miami, FL, U. S.)* **79**, 113s (2000).

<sup>25</sup>C. Huang and S. Kou, *Weld. J. (Miami, FL, U. S.)* **80**, 9s (2001).

<sup>26</sup>C. Huang and S. Kou, *Weld. J. (Miami, FL, U. S.)* **80**, 46s (2001).

<sup>27</sup>C. Huang and S. Kou, *Weld. J. (Miami, FL, U. S.)* **81**, 211s (2002).

<sup>28</sup>C. Huang and S. Kou, *Weld. J. (Miami, FL, U. S.)* **82**, 184s (2003).

<sup>29</sup>C. Huang and S. Kou, *Weld. J. (Miami, FL, U. S.)* **83**, 111s (2004).

<sup>30</sup>S. Kou and Y. H. Wang, *Metall. Trans. A* **17**, 2271 (1986).

<sup>31</sup>S. Chakraborty and P. Dutta, *Mater. Manuf. Processes* **17**, 455 (2002).

<sup>32</sup>A. D. Brent, V. R. Voller, and K. J. Reid, *Numer. Heat Transfer* **13**, 297 (1988).

<sup>33</sup>V. R. Voller, A. D. Brent, and C. Prakash, *Int. J. Heat Mass Transfer* **32**, 1719 (1989).

<sup>34</sup>S. V. Patankar, *Numerical Heat Transfer and Fluid Flow* (Hemisphere/McGraw-Hill, Washington, DC, 1980).

<sup>35</sup>S. Chakraborty and P. Dutta, *Metall. Mater. Trans. B* **32**, 562 (2001).

<sup>36</sup>P. Galenko and S. Sobolev, *Phys. Rev. E* **55**, 343 (1997).

<sup>37</sup>W. Kurz and D. J. Fisher, *Fundamentals of Solidification*, 3rd ed. (Trans. Tech. Publications, Switzerland, 1992).

<sup>38</sup>M. C. Flemings, *Solidification Processing* (McGraw-Hill, New York, 1974).

<sup>39</sup>Q. Z. Diao and H. L. Tsai, *Metall. Trans. A* **24**, 963 (1993).

<sup>40</sup>N. F. Gittos and M. H. Scott, *Weld. J. (Miami, FL, U. S.)* **60**, 95s (1981).